Entanglement with classical fields

K. F. Lee and J. E. Thomas
Physics Department, Duke University, Durham, North Carolina 27708-0305, USA
(Received 19 August 2002; published 13 May 2004)

We experimentally demonstrate a simple classical-field optical heterodyne method which employs postselection to reproduce the polarization correlations of a four-particle entangled state. We give a heuristic argument relating this method to the measurement of multiple quantum fields by correlated homodyne detection. We suggest that using multiple classical fields and postselection, one can reproduce the polarization correlations obtained in quantum experiments which employ multiple single-photon sources and linear optics to prepare multiparticle entangled states. Our experimental scheme produces four spatially separated beams which are separately detected by mixing with four independent optical local oscillators (LO) of variable polarization. Analog multiplication of the four beat signals enables projection onto a four-particle polarization-state basis. Appropriate band pass filtering is used to produce a signal proportional to the projections of the maximally entangled four-field polarization state, $|H_1)|H_2)|H_3)|H_4)+|V_1)|V_2)|V_3)|V_4)$, onto the product of the four LO polarizations. Since the data from multiple observers is combined prior to postselection, this method does not constitute a test of nonlocality. However, we reproduce the polarization correlations of the 32 elements in the truth table from the quantum mechanical Greenberger-Horne-Zeilinger experiments on the violation of local realism. We also demonstrate a form of classical entanglement swapping in a four-particle basis.

DOI: 10.1103/PhysRevA.69.052311 PACS number(s): 03.67.−a, 42.50.−p

I. INTRODUCTION

Currently, there is great interest in understanding what constitutes truly quantum mechanical behavior. This question is of particular significance in the areas of quantum computation, quantum teleportation, and quantum cryptography, where superposition and entanglement play a central role. One way to explore this question is to study the differences and similarities between measurements made on quantum and classical-wave systems [1]. The purpose of the present paper is to present one such study, a demonstration of the entanglement of four classical fields.

Superposition and interference are common to both quantum wave functions and classical waves. As a consequence of interference in a single-particle quantum system, the Wigner phase space function can be negative, as in a quantum superposition of states (Schrödinger cat state). Using a two-window heterodyne detection method, we have demonstrated that the transverse mode of a classical field with two mutually coherent spatially separated lobes also has a Wigner phase-space function with a negative region [2].

A central feature of superposition and interference in multiparticle quantum systems is the concept of entanglement, which describes correlations between the measured properties of different particles, such as their momenta or polarizations [3,4]. The concept of entanglement and a general definition of its measure are currently being explored [5].

In practice, it is difficult to prepare entangled many-particle quantum states. One proposed simplifying method employs single-photon sources and linear optics to overcome this problem [6,7]. As a further simplification, weak-coherent sources and phase modulation are already being employed to implement quantum key distribution employing the BB84 protocol [8,9]. The classical-field methods exploit the fact that the wave function of a single photon in a given spatial mode $\mathcal{E}_l(\mathrm{x})$ is the same as the mode function, i.e., the wave function is $\langle 0|\hat{\mathcal{E}}(\mathrm{x})|1_l\rangle=\mathcal{E}_l(\mathrm{x})$, where $\hat{\mathcal{E}}$ is the positive frequency part of the field operator.

Using photons from independent sources and linear optics [10–12], postselection techniques have been used to demonstrate violations of Bell's inequalities and also to implement quantum logic gates such as a controlled-NOT gate. Further, it has been suggested that the violation of Bell's inequality for continuous variables can be accomplished using macroscopic light fields [13]. Since the mode function $\mathcal{E}_l(\mathrm{x})$ is the same as the transverse mode of a classical field, these ideas suggest that classical fields and linear optics can be used to create entangled states of multiple classical fields by postselection. Indeed, it has been pointed out that postselection techniques allow violation of Bell's inequality even with classical correlations [14]. Our paper is a direct demonstration of this idea.

Study of entanglement with classical fields may offer useful alternatives to entanglement obtained by using photons from independent sources to implement quantum information processing and provides new insights into the fundamental features of quantum measurement and entanglement. Our classical experiments employ heterodyne detection to measure field correlations and postselection by frequency filtering after the data from multiple observers is combined.

Our heterodyne method is similar to the homodyne techniques which have been used previously to measure the nonlocal correlations in a two-particle quantum entangled system, and to demonstrate a violation of Bell's inequalities. In the experiment by Ou *et al.* of Ref. [15], strong local oscillator fields are used for homodyne detection of correlated photon pairs, where correlations between the two detected quadrature field amplitude fluctuations are measured. By contrast, other experiments [16–18] employ weak local oscillator fields, which are used to measure the phase differ-

ences between correlated photon pairs and the local oscillator fields. For weak local oscillator fields, photon counting is employed for the measurements. In homodyne experiments with either weak or strong local oscillator fields, pairs of single-mode correlated fields or two-field correlations are detected via the measured intensity correlations.

Recently, we have demonstrated a classical-wave method for reproducing the correlations of a two-particle entangled state using independent heterodyne measurements on spatially separated beams followed by postselection [19]. In those experiments, polarization correlations are obtained between two spatially separated classical fields. It is shown that Bell's inequalities are formally violated since the interferences of a two-particle entangled quantum state are reproduced. The method combines the data from the two observers by analog multiplication and then uses postselection by frequency filtering to measure the desired part of the interference signal. Since the data from the two observers is combined before postselection, this method does not constitute a test of quantum nonlocality. However, the classical correlations so obtained reproduce those of the corresponding quantum experiments.

A classical-wave method for reproducing the correlations of a three-photon Greenberger-Horne-Zeilinger (GHZ) experiment has been suggested theoretically [1]. The suggested experiment reproduces the correlations that formally violate local realism. However, the proposed method has the property that the measurements made by the three observers cannot be spatially separated, since the interferences occur in the position-polarization entangled state of a single field. Hence, nonlocal correlations cannot be demonstrated. Furthermore, although such experiments can in principle be implemented, as noted in Ref. [1], they have not been done.

In this paper, we demonstrate a simple classical-wave experiment which employs postselection to reproduce the polarization correlations of three- and four-particle entangled states. In contrast to the schemes suggested in Ref. [1], our technique does not require phase stability of interfering beams. In our work, four spatially separated classical beams, 1–4, each containing two orthogonally polarized fields with different frequencies, are used to measure the four-field polarization entangled state $|\Psi_{cl}) = [|H_1)|H_2)|H_3)|H_4) + |V_1)|V_2)|V_3)|V_4)]/\sqrt{2}$, where we use the parenthesis notation of Spreeuw to denote the classical polarization state [20]. The classically correlated state is directly measured by heterodyne detection with four independent local oscillator (LO) beams of arbitrary polarizations, using a scheme which is independent of the LO phases to obtain stable signals. By fixing the polarization of the fourth LO beam at 45°, our classical system reproduces the correlations obtained for a three-particle GHZ entanglement [21,22]. To demonstrate the correlation properties of the classical field GHZ state, we reproduce the 32 elements of the truth table which is used in the quantum experiments to demonstrate violation of local realism.

The central feature of our scheme is the use of heterodyne detection of multiple classical fields. The detection system employs analog multiplication of the signals from several observers and subsequent frequency selection (instead of coincidence detection) to postproject the desired entangled part of the four-field state. Since the method combines the data from several observers before postselection, it cannot be used to test nonlocality. However, the method does yield a signal proportional to the inner product of a chosen multiparticle entangled state onto the product basis of the multiple field polarization states. The square of the signal amplitude so obtained is proportional to the joint probability for the corresponding quantum experiment.

Briefly, to produce a four-field entangled state, we employ an optical beam of frequency $\omega_v = \omega + 2\pi \times 120$ kHz with vertical polarization and an optical beam of frequency $\omega_H = \omega + 2\pi \times 30$ kHz with horizontal polarization, which are combined through a 50/50 beamsplitter. Two additional beamsplitters, placed at the outputs of the first, produce four spatially separated superposition beams. Two of these beams are rotated in polarization using a half-wave plate at a 45° angle to interchange the horizontal and vertical components. The four output beams are sent to four spatially separated measurement systems, each of which employs heterodyne detection with an independent LO of frequency ω and at arbitrary polarization angle. The heterodyne signal at each detector then contains two frequency components, at 30 and 120 kHz. Correlated field detection is accomplished by using three analog multipliers to produce a four-field product signal. The number of multipliers is equal to the number of coincidence detectors required in a quantum experiment. Band pass filtering after each multiplier is used to select the components of the desired state, yielding an overall signal at 300 kHz that contains two indistinguishable, interfering contributions, proportional to the projections of the four-field state $|H_1)|H_2)|H_3)|H_4) + |V_1)|V_2)|V_3|V_4)$ onto the product of the four LO polarizations.

We begin by giving a heuristic argument in Sec. II which relates our classical-field heterodyne method to the correlated homodyne detection of multiple fields in quantum experiments and to the measurement of the corresponding quantum intensity correlations. In Sec. III, we describe our previous experiments which reproduce the polarization correlations obtained in the coincidence detection of entangled two-particle states [19]. In later sections, this technique is extended to reproduce the correlations obtained in fourfold coincidence detection. To demonstrate the correlation properties of the classical-field state, measurements are made in the same basis as employed for the GHZ test of local realism. For this reason, in Sec. IV, we briefly review the quantum test of local realism for three-particle GHZ entanglement [21,22]. In Sec. V, we demonstrate that the classical-field experiments reproduce the 32 elements of the truth table obtained in quantum experiments on a three-particle GHZ entangled state, which contradicts local realism. As an application of our four-field entangled state, we briefly demonstrate a classical version of entanglement swapping in Sec. VI.

II. QUANTUM INTENSITY CORRELATIONS AS A CONSEQUENCE OF CORRELATED FIELDS

Homodyne detection of quantum correlated optical beams has previously been explored as a means of demonstrating

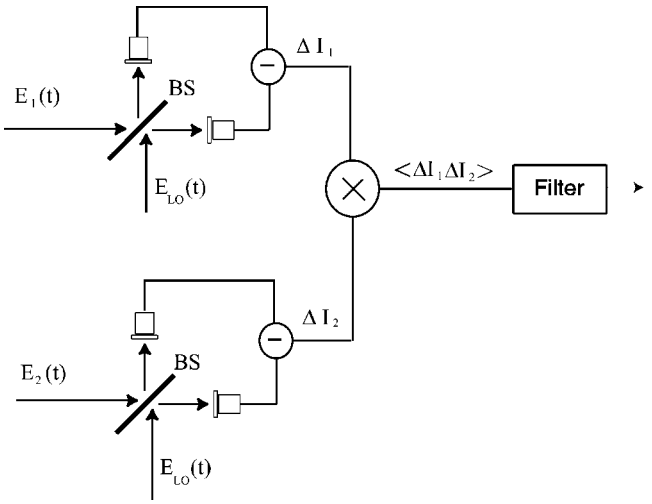

FIG. 1. Correlated homodyne detection of two fields. Fluctuations in the quantum field $E_1(t)$ are measured by mixing with a strong classical local oscillator (LO) field $E_{LO}(t)$ using a balanced detection scheme. Using an independent LO field, fluctuations in the field $E_2(t)$ are measured. The product of the fluctuating currents ΔI_1 and ΔI_2 yields the correlation between the fluctuations in the quantum fields 1 and 2.

the violation of Bell's inequalties [16–18]. In this section, we give a heuristic argument to show that the correlated detection of photons in two separated beams can be interpreted as arising from correlated fluctuations in their respective field operators which are directly measurable via homodyne detection as shown in Fig. 1. The fields are correlated at the source and propagate causally to the separated observers. This concept of correlated field fluctuations shows how the correlations measured in quantum intensity correlation experiments can be reproduced by measuring the product of homodyne or heterodyne detection signals, which measure the field.

Typical two-photon sources are based on parametric downconversion. In the Mandel-Ou experiments [3], a type II downconverter produces a pair of orthogonally polarized photons which are combined on a beam splitter. We assume that for each pump pulse, the probability $|\epsilon|^2$ of creating the two-photon state is small so that photon pile up is avoided. Following the pump pulse, the quantum state of the fields in output ports 1 and 2 of the beam splitter then can be written as

$$|\Psi\rangle = |\text{vac}\rangle + \frac{\epsilon}{2}[(|H_1V_2\rangle - |V_1H_2\rangle) + (|H_1V_1\rangle - |H_2V_2\rangle)]. \tag{1}$$

Here, the first term is the vacuum state with no photons present, while the two-photon state contains states for the orthogonally polarized photons to be split between the two beams or to both go into one beam or the other.

In the experiments, polarizers are placed in each beam and oriented at angles θ_1 and θ_2, respectively. The field operator after polarizer 1 is $\mathcal{E}_1 = \cos\,\theta_1\, a_{1H} + \sin\,\theta_1\, a_{1V}$, where $a_{1H}(a_{1V})$ is the annihilation operator for a horizontally (vertically) polarized photon in beam 1. Similarly, for polarizer 2, $\mathcal{E}_2 = \cos\,\theta_2\, a_{2H} + \sin\,\theta_2\, a_{2V}$.

For intensity correlation (photon coincidence) measurement, one measures the operator I_1I_2, where $I_{1,2} \propto \mathcal{E}_{1,2}^{\dagger}\,\mathcal{E}_{1,2}$. In this case, neither the vacuum state nor the states with both photons in one beam contribute to the coincidence probability. The coincidence intensity measurement postprojects out the desired part of the quantum state and the relative probability of coincidence is $\langle\Psi|I_1I_2|\Psi\rangle = (\epsilon/2)^2 \sin^2(\theta_2 - \theta_1)$. The probability for detecting a photon in either beam is the same as the probability of pair production, and is $\langle\Psi|I_1|\Psi\rangle = \langle\Psi|I_2|\Psi\rangle = \epsilon^2/2$. The corresponding probability of coincidence is then $\langle\Psi|I_1I_2|\Psi\rangle / \langle\Psi|I_1|\Psi\rangle = \sin^2(\theta_2 - \theta_1)/2$.

As noted above, to guarantee that only two photons are prepared and detected in each measurement, the production and the detection rate of pairs is low and $|\epsilon|^2 \ll 1$. Hence, the quantum state of Eq. (1) is mostly the vacuum state. Nevertheless, the vacuum state plays no role in the calculation of the coincidence probability and it is usually omitted in describing the state.

However, the vacuum state leads to correlated field fluctuations. Since $\langle\Psi|\mathcal{E}_{1,2}|\Psi\rangle = 0$, the mean fields are zero, although the corresponding intensities are nonzero. Hence, the fields can be considered to fluctuate. The field fluctuations are correlated since $\langle\Psi|\mathcal{E}_2\mathcal{E}_1|\Psi\rangle = \epsilon\,\sin(\theta_2 - \theta_1)/2 \neq 0$. Hence, the nonlocal intensity correlations measured by the two detectors can be considered to arise from correlations in the field fluctuations. A field fluctuation in one detector is polarization correlated with a field fluctuation in the other.

When the mean fields are nonzero, one can consider a measurement of a fluctuation in one detector to determine the relative phase between the field fluctuation and the mean field in that detector. Since the mean fields and the field fluctuations are correlated at the source, this necessarily determines the correlation between the mean field and field fluctuation in the other detector. These field correlations are built in at the source and propagate causally to the two observers according to Maxwell's equations.

An important property of multiparticle states which take the form of Eq. (1) is that

$$\langle\Psi|I_1I_2|\Psi\rangle = |\langle\Psi|\mathcal{E}_2\mathcal{E}_1|\Psi\rangle|^2. \tag{2}$$

Equation (2) shows that the same correlations obtained by joint intensity measurement can be obtained by correlated field measurement. In principle, this can be accomplished by homodyne detection of each field as used previously to measure the Wigner function for a single mode field [23]. In this case, Fig. 1, a balanced detection system 1 would measure a signal proportional to $V_1 = \mathcal{E}_{LO1}^{*}\,\mathcal{E}_1 + \text{H.c.}$, where the LO field is a strong classical field, and similarly for balanced detector 2. Multiplication of the homodyne signals for two balanced detectors, squaring, and averaging over the classical phases of the local oscillator fields yields a result proportional to the right-hand side of Eq. (2).

Equation (2) explains why the measurement of correlated classical fields can reproduce quantum correlation measurements. As demonstrated below, we use a product of signals from multiple heterodyne detectors to obtain a signal proportional to the product of the classical-field amplitudes. With appropriate band pass filtering, we postproject only that part of the signal proportional to the entangled state of interest. By defining the joint intensity to be proportional to the square of the product of the heterodyne signals, according to Eq. (2), one obtains polarization correlations in agreement with the quantum results [19].

III. TWO-PARTICLE ENTANGLEMENT

In quantum optics, coincidence detection yields the joint probability of an event and also acts as a projection measurement on the desired quantum state in a multiparticle system, eliminating for example, the vacuum state as described above. In a two-photon system described in abbreviated form by an entangled state

$$|\psi^-\rangle = (|H_1V_2\rangle - |V_1H_2\rangle)/\sqrt{2},$$

these two photons are produced by parametric downconversion. They are orthogonally polarized signal and idler photons, which are combined with a beamsplitter [3]. The outputs of the beamsplitter provide two spatially separated beams, beams 1 and 2 which propagate to two analyzers. Beam 1 propagates to an analyzing linear polarizer at an angle θ_1, with respect to the horizontal axis. The analyzer projects out the polarization component

$$|\theta_1\rangle = \cos\ \theta_1|H_1\rangle + \sin\ \theta_1|V_1\rangle. \tag{3}$$

Similarly, beam 2 propagates to analyzer 2 which projects out the polarization component

$$|\theta_2\rangle = \cos\ \theta_2|H_2\rangle + \sin\ \theta_2|V_2\rangle. \tag{4}$$

Now, by detecting these two photons in coincidence, we obtain the joint probability $P(\theta_1, \theta_2)$ for the detection of one photon of polarization θ_1 and one photon of polarization θ_2 as

$$P(\theta_1, \theta_2) = |\langle\theta_1, \theta_2|\psi^-\rangle|^2 = \frac{1}{2}\sin^2(\theta_1 - \theta_2). \tag{5}$$

From Eq. (5), coincidence detection projects the entangled state $|\psi^-\rangle$ onto the product state $|\theta_1\rangle|\theta_2\rangle$.

These joint detection probabilities can be reproduced by using two classical fields [19]. In the classical-field experiments, frequency selection rather than time domain coincidence is used to postproject the desired part of the multiparticle quantum state. Two optical beams with fields $|1\rangle$, $|2\rangle$ are each generated by combining on a beamsplitter a field of frequency $\omega+\delta_H$ with horizontal polarization and a field of frequency $\omega+\delta_V$ with vertical polarization. Fields $|1\rangle$ and $|2\rangle$ are each measured by heterodyne detection using a LO of frequency ω with variable polarization, yielding two beat signals each containing two frequencies, δ_H and δ_V. An analog multiplier is used to obtain the product of the beat signals from each detector, producing a net signal amplitude that is proportional to the projection of a factorized input field state $|1\rangle|2\rangle$ onto the two-field polarization state $|\theta_1\rangle|\theta_2\rangle$ of the LO's. A band pass filter at the frequency $\delta_H+\delta_V$ is then used to postproject a signal containing two interfering contributions, which is proportional to the inner product of $|\psi_{cl}^-\rangle=[|H_1\rangle|V_2\rangle-|V_1\rangle|H_2\rangle]/\sqrt{2}$ onto the LO polarization state $|\theta_1\theta_2\rangle$. The square of the amplitude of this signal is proportional to the joint probability of Eq. (5). The present paper extends this method to produce four-field entanglement, reproducing the truth table for the GHZ test of local realism.

IV. CORRELATIONS IN GHZ ENTANGLEMENT

In our experiments, we produce a classical four-field entangled state. To demonstrate that the classical state produces the same polarization correlations as the true quantum state, it is convenient to use the same methods and the same basis states as in the GHZ test of local realism theory.

We begin by reviewing the essential features of the GHZ test of local realism theory that is based on a quantum mechanical three-particle entangled state [21,22]. The preparation of entangled states of three or more particles is experimentally challenging. In the experiment of three-particle entanglement demonstrated by Zeilinger's group [24], two pairs of polarization entangled photons are transformed into three entangled photons and a fourth independent photon. The fourfold coincidence detection of these four photons provides a projection measurement onto the desired GHZ state $|\psi\rangle=(1/\sqrt{2})(|H_1\rangle|H_2\rangle|V_3\rangle+|V_1\rangle|V_2\rangle|H_3\rangle)|H_4\rangle$. The fourth photon $|H_4\rangle$ is a trigger photon and the remaining three entangled photons are used to observe the GHZ entanglement. The fourth photon is always horizontally polarized and hence can be neglected in determining the states of the remaining three photons. By rotating the third-photon polarization state so that the horizontal and vertical components are interchanged, i.e., $V_3\leftrightarrow H_3$, any measurement on the first three particles in the state $|\psi\rangle$ can be regarded as a measurement on the three-particle GHZ entangled state,

$$|\Psi_{GHZ}^3\rangle = \frac{1}{\sqrt{2}}(|H_1\rangle|H_2\rangle|H_3\rangle + |V_1\rangle|V_2\rangle|V_3\rangle). \tag{6}$$

Here the superscript 3 indicates a three-photon state. The GHZ arguments about physical reality are based on the measurements of polarization correlations on three particles in this GHZ state. The measurements of polarization correlations between the three particles leads to a conflict with local realism for nonstatistical predictions of quantum mechanics [21,22]. That is in contrast to the two entangled particles test of Bell's inequalities, where the conflict arises for statistical predictions of quantum mechanics.

We can demonstrate the GHZ argument [21,22] for a three-particle test of local realism as follows: A photon *i* is

said to possess an element of reality X_i with the value +1 or −1 when its linear polarization state is H' or V', respectively, where H' and V' are at angles 45° and −45° with respect to the original vertical direction V. Similarly, a photon is said to possess an element of reality Y_i with value +1 or −1 when its polarization state is right handed, R, or left handed, L, respectively. The polarization states corresponding to these elements of reality are given by

$$\begin{aligned} |H'\rangle &= \frac{1}{\sqrt{2}}(|H\rangle + |V\rangle), \\ |V'\rangle &= \frac{1}{\sqrt{2}}(|H\rangle - |V\rangle), \\ |R\rangle &= \frac{1}{\sqrt{2}}(|H\rangle + i|V\rangle), \\ |L\rangle &= \frac{1}{\sqrt{2}}(|H\rangle - i|V\rangle), \end{aligned} \tag{7}$$

where the $H(V)$ is the horizontal (vertical) polarization state of the photon.

One can define elements of reality for joint measurement of three particles as the product of the elements of reality for each particle. For example, a measurement $Y_1Y_2X_3$ on the GHZ state means that the first and second photons are each projected onto the polarization state $|R\rangle$ or $|L\rangle$, and the third photon is projected onto the polarization state $|H'\rangle$ or $|V'\rangle$. Since each of the photons has two orthogonal polarizations in the chosen basis, there is a complete set of $2^3=8$ orthogonal three-photon product states in this measurement. There are also eight possible combinations for measuring either circular Y or linear X polarization on three particles, and eight possible three-photon states for each combination. In the following, we consider four types of measurements for the GHZ state of Eq. (6), namely $Y_1Y_2X_3$, $Y_1X_2Y_3$, and $X_1Y_2Y_3$, and $X_1X_2X_3$.

In order to determine which elements of reality for three-photon coincidences are also realizations predicted by quantum mechanics, we conduct measurements on polarization correlations of three photons in the GHZ state. Suppose now that certain measurements of $Y_1Y_2X_3$, $Y_1X_2Y_3$, and $X_1Y_2Y_3$ are predicted to be nonzero for the GHZ state. Then for an $X_1X_2X_3$ experiment, the expectations using a local realistic theory are exactly the opposite of the expectations using quantum physics, as we now show, following the arguments of Refs. [21,22].

To see why, let's demonstrate the argument with an example for the measurement combination $Y_1Y_2X_3$ on the GHZ state. We write Eq. (6) in a form which directly shows the possible outcomes for $Y_1Y_2X_3$ measurements. For the three photons, the polarizations $|R_1\rangle$, $|L_1\rangle$, $|R_2\rangle$, $|L_2\rangle$, $|H_3'\rangle$, and $|V_3'\rangle$ are obtained from Eq. (7). Then, the states $|H_i\rangle$ and $|V_i\rangle$, where $i=1,2,3$, can be written in the measurement basis as

$$\begin{aligned} |H_1\rangle &= \frac{1}{\sqrt{2}}(|R_1\rangle + |L_1\rangle), \\ |V_1\rangle &= \frac{1}{i\sqrt{2}}(|R_1\rangle - |L_1\rangle), \\ |H_2\rangle &= \frac{1}{\sqrt{2}}(|R_2\rangle + |L_2\rangle), \\ |V_2\rangle &= \frac{1}{i\sqrt{2}}(|R_2\rangle - |L_2\rangle), \\ |H_3\rangle &= \frac{1}{\sqrt{2}}(|H_3'\rangle + |V_3'\rangle), \\ |V_3\rangle &= \frac{1}{\sqrt{2}}(|H_3'\rangle - |V_3'\rangle). \end{aligned} \tag{8}$$

Now, by using the Eq. (8) for three photons in the GHZ state, $|\Psi_{GHZ}^3\rangle$ of Eq. (6) can be rewritten in the basis for the YYX configuration as

$$|\Psi_{GHZ}^3\rangle_{YYX} = \frac{1}{2}(|R_1L_2H_3'\rangle + |L_1R_2H_3'\rangle + |R_1R_2V_3'\rangle + |L_1L_2V_3'\rangle). \tag{9}$$

One can see that each three-particle state of Eq. (9) has an element of reality $Y_1Y_2X_3$ with a product value of −1. Note that the $R_1L_2H_3'=-1$ means that if the photon 1 is R polarized and photon 2 is also L polarized, then, the photon 3 must be H' polarized. The existence of the component $|R_1\rangle|L_2\rangle|H_3'\rangle$ and not of its complementary component $|R_1\rangle|L_2\rangle|V_3'\rangle$ can also be verified by direct projection on the GHZ state $|\Psi_{GHZ}^3\rangle$, i.e., $\langle R_1|\langle L_2|\langle H_3'|\Psi_{GHZ}^3\rangle = 1/2$ and $\langle R_1|\langle L_2|\langle V_3'|\Psi_{GHZ}^3\rangle = 0$. Thus, in the measurement $Y_1Y_2X_3$, four of eight possible components of three-photon product states are nonzero for the GHZ state. By using the same procedure as discussed above for the YYX configuration, the GHZ state can be written to display the YXY, XYY, and XXX configurations of reality by using the appropriate basis,

$$|\Psi_{GHZ}^3\rangle_{YXY} = \frac{1}{2}(|L_1H_2'R_3\rangle + |R_1V_2'R_3\rangle + |R_1H_2'L_3\rangle + |L_1V_2'L_3\rangle), \tag{10}$$

$$|\Psi_{GHZ}^3\rangle_{XYY} = \frac{1}{2}(|H_1'L_2R_3\rangle + |V_1'R_2R_3\rangle + |H_1'R_2L_3\rangle + |V_1'L_2L_3\rangle), \tag{11}$$

and

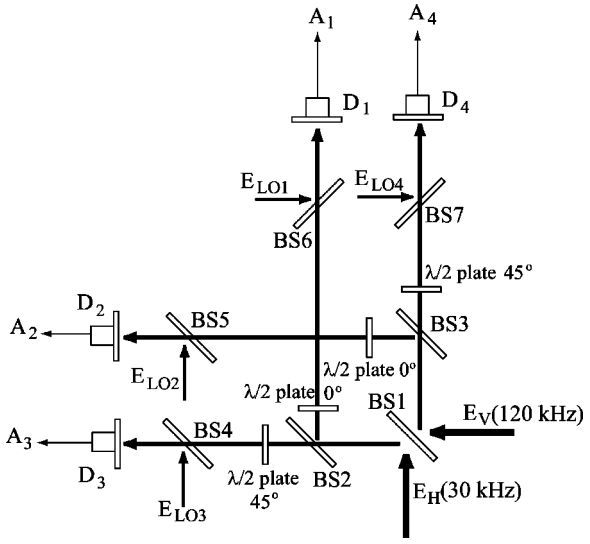

FIG. 2. Experimental arrangement for the measurement of the four-field entangled state $|\Psi_{cl}^4\rangle_{GHZ}$. D_1, D_2, D_3, and D_4 are detectors used to obtain the beat signal amplitudes A_1, A_2, A_3, and A_4 respectively, each of which contains two frequencies, 120 and 30 kHz.

$$|\Psi_{GHZ}^3\rangle_{XXX} = \frac{1}{2}(|H_1'H_2'H_3'\rangle + |V_1'V_2'H_3'\rangle + |H_1'V_2'V_3'\rangle + |V_1'H_2'V_3'\rangle). \tag{12}$$

As in Eq. (9) for the *YYX* configuration, each element of reality for the three photons in the configurations $X_1Y_2Y_3$ of Eq. (10) and $Y_1X_2Y_3$ of Eq. (11) has the product value of -1.

Now, according to the local realism theory, since $Y_iY_i=+1$, it is obvious that the product of three configurations $[(X_1Y_2Y_3)(Y_1X_2Y_3)(Y_1Y_2X_3)]=X_1X_2X_3$ will lead to the prediction that $X_1X_2X_3=-1$, since each factor is -1 according to the above arguments. However, this is in contradiction with the quantum results obtained directly from Eq. (12) for the GHZ state in the $X_1X_2X_3$ basis, where $X_1X_2X_3=+1$.

In the following section, we describe a classical experiment which measures the four-field entangled state $[|H_1H_2H_3H_4\rangle+|V_1V_2V_3V_4\rangle]\sqrt{2}$. As in the quantum experiments, we use this state to measure the correlations for the three-particle GHZ state of Eq. (6). To verify the polarization correlations in the classical state, we reproduce the results predicted by quantum mechanics in the test of quantum nonlocality.

V. REPRODUCING GHZ ENTANGLEMENT WITH CLASSICAL FIELDS

In our experiments, as seen in Fig. 2, a HeNe laser beam is split and sent through two fixed-frequency acousto-optic modulators to produce a beam of frequency $\omega_H=\omega+\delta_H$ with horizontal polarization and a beam of frequency $\omega_v=\omega+\delta_V$ with vertical polarization, where $\delta_H=2\pi\times 30$ kHz and $\delta_V=2\pi\times 120$ kHz. These two beams are combined on beam splitter BS1 producing two output fields. Beamsplitter BS2 produces two copies of the transverse mode of one of the output fields of BS1: beam 1, which propagates to detector 1 and beam 3, which propagates to detector 3. Similarly, beamsplitter BS3 produces two copies of the transverse mode of the other output field of BS1: beam 2 propagates to detector 2 and beam 4 propagates to detector 4. Half-wave plates oriented at 0° in beams 1 and 2 shift the phase of the horizontal field relative to that of the vertical. This cancels the 180° relative phase shifts arising from BS1. The total fields $\mathbf{E}_1$ and $\mathbf{E}_2$ in beams 1 and 2, respectively, are then given by

$$\mathbf{E}_1 = \mathcal{E}_1 \exp(-i\omega_V t)\hat{V}_1 + \mathcal{E}_1 \exp(-i\omega_H t)\hat{H}_1, \tag{13}$$

$$\mathbf{E}_2 = \mathcal{E}_2 \exp(-i\omega_V t)\hat{V}_2 + \mathcal{E}_2 \exp(-i\omega_H t)\hat{H}_2. \tag{14}$$

Half-wave plates oriented at 45° in beams 3 and 4 interchange the horizontal and vertical components. The optical fields $\mathbf{E}_3$ and $\mathbf{E}_4$ are given by

$$\mathbf{E}_3 = \mathcal{E}_3 \exp(-i\omega_H t)\hat{V}_3 + \mathcal{E}_3 \exp(-i\omega_V t)\hat{H}_3, \tag{15}$$

$$\mathbf{E}_4 = \mathcal{E}_4 \exp(-i\omega_H t)\hat{V}_4 + \mathcal{E}_4 \exp(-i\omega_V t)\hat{H}_4. \tag{16}$$

Each of the four beams is sent to a heterodyne detector and mixed with an independent local oscillator beam of frequency ω. The relative phases of the local oscillators are independent and not stabilized. As shown below, the local oscillator phases appear as a common factor in the signals and therefore do not need to be controlled. The polarization state of each local oscillator beam is chosen to be in one of the four polarizations H', V', R, and L by using a $\lambda/2$ plate and a $\lambda/4$ plate independently.

Now, in order to demonstrate that our classical-field system can reproduce projection measurements on the GHZ state of Eq. (6), we choose the four local oscillator beams at arbitrary polarization angles with unit vectors denoted by $\hat{\mathbf{e}}_{LOi}$, where $i=1,2,3,4$. The heterodyne beat signal is detected as shown in the detection diagram of Fig. 3. In detector D_1, the amplitude of the heterodyne beat signal obtained from the interference between local oscillator LO1 and the field $\mathbf{E}_1$ can be written in the parenthesis notation of Ref. [20],

$$A_1 = (\mathbf{E}_{LO1}|\mathbf{E}_1) \equiv \int dxdy\, E_{LO1}^*(x,y,t)\hat{\mathbf{e}}_{LO1}^* \cdot \mathbf{E}_1(x,y,t), \tag{17}$$

and similarly for LO2, LO3, and LO4. Here, $E_{LO1}(x,y,t)=\mathcal{E}_{LO1}(x,y)\exp(-i\omega t)$ is the LO1 field amplitude in the plane of a photodiode detector and $\mathbf{E}_1$ is the vector field amplitude for beam 1. By using Eq. (13), the beat signal amplitude A_1 is then

$$A_1 \propto (\hat{\mathbf{e}}_{LO1}|\hat{\mathbf{V}}_1)(\mathcal{E}_{LO1}|\mathcal{E}_1)\exp(-i\delta_V t) + (\hat{\mathbf{e}}_{LO1}|\hat{\mathbf{H}}_1)(\mathcal{E}_{LO1}|\mathcal{E}_1)\exp(-i\delta_H t), \tag{18}$$

where $(\mathcal{E}_{LO1}|\mathcal{E}_1)$ denotes the spatial overlap integral of LO1 and the field of beam 1. The beat signal amplitudes in detectors D_2, D_3, and D_4 are similarly given by

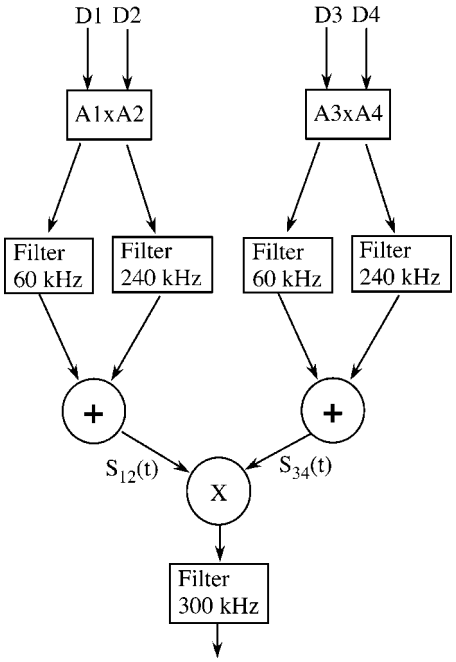

FIG. 3. Detection scheme for observing GHZ entanglement by frequency postselection. The analog multipliers (×), band pass filters, and summing amplifiers (+) enable postprojection of an entangled four-field state onto a four-field product basis.

$$A_2 = (\mathbf{E}_{LO2}|\mathbf{E}_2) \propto (\hat{\mathbf{e}}_{LO2}|\hat{\mathbf{V}}_2)(\mathcal{E}_{LO2}|\mathcal{E}_2)\exp(-i\delta_V t) + (\hat{\mathbf{e}}_{LO2}|\hat{\mathbf{H}}_2) \times (\mathcal{E}_{LO2}|\mathcal{E}_2)\exp(-i\delta_H t),$$

$$A_3 = (\mathbf{E}_{LO3}|\mathbf{E}_3) \propto (\hat{\mathbf{e}}_{LO3}|\hat{\mathbf{V}}_3)(\mathcal{E}_{LO3}|\mathcal{E}_3)\exp(-i\delta_H t) + (\hat{\mathbf{e}}_{LO3}|\hat{\mathbf{H}}_2) \times (\mathcal{E}_{LO3}|\mathcal{E}_3)\exp(-i\delta_V t),$$

$$A_4 = (\mathbf{E}_{LO4}|\mathbf{E}_4) \propto (\hat{\mathbf{e}}_{LO4}|\hat{\mathbf{V}}_4)(\mathcal{E}_{LO4}|\mathcal{E}_4)\exp(-i\delta_H t) + (\hat{\mathbf{e}}_{LO4}|\hat{\mathbf{H}}_4) \times (\mathcal{E}_{LO4}|\mathcal{E}_4)\exp(-i\delta_V t). \quad (19)$$

As shown in the detection diagram, Fig. 3, the beat signals from detectors D_1 and D_2 are sent to an analog multiplier which yields a product signal $(A_1+A_1^*)(A_2+A_2^*)$ proportional to the real part of the amplitude $A_1A_2+A_1^*A_2$. The beat amplitudes A_1 and A_2 each contain two beat frequencies δ_H and δ_V, yielding nonzero frequency components in the product signal: $\delta_H \pm \delta_V$, $2\delta_H = 60$ kHz, and $2\delta_V = 240$ kHz. Bandpass filters are used to select the product signals at the sum frequencies $2\delta_H$ and $2\delta_V$. In this case, only one part of the product amplitude, i.e., A_1A_2, contributes to the bandpassed signal. The corresponding beat signal amplitudes are, respectively,

$$\gamma_{60\ \mathrm{kHz}}(A_1,A_2) \propto (\mathcal{E}_{LO1}|\mathcal{E}_1)(\mathcal{E}_{LO2}|\mathcal{E}_2)(\hat{\mathbf{e}}_{LO1}|\hat{\mathbf{H}}_1)(\hat{\mathbf{e}}_{LO2}|\hat{\mathbf{H}}_2) \quad (20)$$

and

$$\gamma_{240\ \mathrm{kHz}}(A_1,A_2) \propto (\mathcal{E}_{LO1}|\mathcal{E}_1)(\mathcal{E}_{LO2}|\mathcal{E}_2)(\hat{\mathbf{e}}_{LO1}|\hat{\mathbf{V}}_1)(\hat{\mathbf{e}}_{LO2}|\hat{\mathbf{V}}_2). \quad (21)$$

The product signals at 60 and at 240 kHz are added by using a summing amplifier, yielding a net signal amplitude $S_{12}(t)$ which contains two contributions, i.e., the $\hat{\mathbf{H}}_1\hat{\mathbf{H}}_2$ component at 60 kHz and the $\hat{\mathbf{V}}_1\hat{\mathbf{V}}_2$ component at 240 kHz.

Similarly, the beat signals from detectors D_3 and D_4 are multiplied, band passed at 60 and 240 kHz. In this case, only the A_3A_4 amplitude contributes to the sum frequency terms. The resulting product signal contains components at 60 and 240 kHz given by

$$\gamma_{60\ \mathrm{kHz}}(A_3,A_4) \propto (\mathcal{E}_{LO3}|\mathcal{E}_3)(\mathcal{E}_{LO4}|\mathcal{E}_4)(\hat{\mathbf{e}}_{LO3}|\hat{\mathbf{V}}_3)(\hat{\mathbf{e}}_{LO4}|\hat{\mathbf{V}}_4) \quad (22)$$

and

$$\gamma_{240\ \mathrm{kHz}}(A_3,A_4) \propto (\mathcal{E}_{LO3}|\mathcal{E}_3)(\mathcal{E}_{LO4}|\mathcal{E}_4)(\hat{\mathbf{e}}_{LO3}|\hat{\mathbf{H}}_3)(\hat{\mathbf{e}}_{LO4}|\hat{\mathbf{H}}_4). \quad (23)$$

Note that horizontal and vertical polarizations are interchanged with respect to Eq. (20). These product signals are added using a summing amplifier, yielding a net signal amplitude $S_{34}(t)$ containing two contributions, i.e., the $\hat{\mathbf{V}}_3\hat{\mathbf{V}}_4$ component at 60 kHz and the $\hat{\mathbf{H}}_3\hat{\mathbf{H}}_4$ component at 240 kHz.

Now, the summed product signals $S_{12}(t)$ and $S_{34}(t)$ are multiplied using an analog multiplier and then band pass filtered at 300 kHz. In this case, the resulting product signal amplitude at 300 kHz contains two interfering contributions, which arise from the two ways that a product of the 60 and 240 kHz components can be obtained:

$$\gamma_{300\ \mathrm{kHz}}(A_1,A_2,A_3,A_4) \propto (\mathcal{E}_{LO1}|\mathcal{E}_1)(\mathcal{E}_{LO2}|\mathcal{E}_2)(\mathcal{E}_{LO3}|\mathcal{E}_3)(\mathcal{E}_{LO4}|\mathcal{E}_4) \times [(\hat{\mathbf{e}}_{LO1}|\hat{\mathbf{V}}_1)(\hat{\mathbf{e}}_{LO2}|\hat{\mathbf{V}}_2)(\hat{\mathbf{e}}_{LO3}|\hat{\mathbf{V}}_3)(\hat{\mathbf{e}}_{LO4}|\hat{\mathbf{V}}_4) + (\hat{\mathbf{e}}_{LO1}|\hat{\mathbf{H}}_1)(\hat{\mathbf{e}}_{LO2}|\hat{\mathbf{H}}_2)(\hat{\mathbf{e}}_{LO3}|\hat{\mathbf{H}}_3)(\hat{\mathbf{e}}_{LO4}|\hat{\mathbf{H}}_4)]. \quad (24)$$

The magnitude of $(\mathcal{E}_{LO1}|\mathcal{E}_1)(\mathcal{E}_{LO2}|\mathcal{E}_2)(\mathcal{E}_{LO3}|\mathcal{E}_3)(\mathcal{E}_{LO4}|\mathcal{E}_4)$ is a common factor in each path and it is controlled by a gain amplifier after each band pass filter. Hence, the product amplitude $\gamma_{300\ \mathrm{kHz}}$ in Eq. (24) can be written as

$$\gamma_{300\ \mathrm{kHz}} \propto (\hat{\mathbf{e}}_{LO1}|(\hat{\mathbf{e}}_{LO2}|(\hat{\mathbf{e}}_{LO3}|(\hat{\mathbf{e}}_{LO4}|\Psi^4_{GHZ})_{cl}, \quad (25)$$

where the $|\Psi^4_{GHZ})_{cl}$ is given by

$$|\Psi^4_{GHZ})_{cl} = \frac{1}{\sqrt{2}}[|H_1H_2H_3H_4) + |V_1V_2V_3V_4)]. \quad (26)$$

Here for simplicity $\hat{H}$ and $\hat{V}$ are denoted as H and V, respectively. The superscript 4 denotes the four-field entangled state. The detection technique projects out the fourfold coincidence signal from the desired entangled four-particle GHZ state. The method measures the projected amplitude, which

can be squared to yield a signal proportional to the fourfold joint intensity.

Now, in order to demonstrate the polarization correlations of the classical four-field state $|\Psi^4_{GHZ}\rangle_{cl}$, we reproduce the correlations for GHZ entanglement by using the three-particle GHZ state. As in the quantum experiments, we fix the polarization of LO4, in our case at 45°,

$$\hat{\mathbf{e}}^{45^\circ}_{LO4} = \frac{1}{\sqrt{2}}(\hat{H}_4 + \hat{V}_4), \tag{27}$$

so that the beat signal A_4 at detector D_4 is equivalent to the trigger photon in the quantum GHZ experiment. Then, $(\hat{e}_{LO4}|\Psi^4_{GHZ})_{cl}$ is proportional to $|H_1H_2H_3\rangle + |V_1V_2V_3\rangle$, that is to $|\Psi^3_{GHZ}\rangle_{cl}$, where the superscript 3 indicates the three-field state. Thus, in the following sections, the frequency filtered signal amplitude at 300 kHz can be used to reproduce the polarization correlations of three-particle GHZ entanglement where the polarizations of LO1, LO2, and LO3 are in one of the four projections, H', V', R, and L.

A. Measurement of the *YYX*, *YXY*, and *XYY* configurations

As a first demonstration of our classical system, we reproduce the polarization correlations for the $Y_1Y_2X_3$ configuration for three-particle GHZ entanglement. As noted above, the LO4 polarization is fixed at 45°, Eq. (27). The possible polarization states of the local oscillator beams LO1, LO2, and LO3 are given by

$$\begin{aligned}
\hat{\mathbf{e}}^{R,L}_{LO1} &= \frac{1}{\sqrt{2}}(\hat{H}_1 \pm i\hat{V}_1),\\
\hat{\mathbf{e}}^{R,L}_{LO2} &= \frac{1}{\sqrt{2}}(\hat{H}_2 \pm i\hat{V}_2),\\
\hat{\mathbf{e}}^{H',V'}_{LO3} &= \frac{1}{\sqrt{2}}(\hat{H}_3 \pm \hat{V}_3).
\end{aligned} \tag{28}$$

For the classical-field state, the measurement of the element of reality $R_1L_2H'_3$ in the $Y_1Y_2X_3$ configuration is accomplished by setting the polarizations of the LO1, LO2, and LO3 beams to be $\hat{\mathbf{e}}^R_{LO1}$, $\hat{\mathbf{e}}^L_{LO2}$, and $\hat{\mathbf{e}}^{H'}_{LO3}$. Now, from Eq. (25) the magnitude of the beat signal γ_{300} kHz is

$$\begin{aligned}
&\gamma_{300\ \mathrm{kHz}}(A_1,A_2,A_3,A_4)\\
&\quad\propto (\hat{\mathbf{e}}^R_{LO1},\hat{\mathbf{e}}^L_{LO2},\hat{\mathbf{e}}^{H'}_{LO3},\hat{\mathbf{e}}^{45^\circ}_{LO4}|\Psi^4_{GHZ})_{cl}\\
&\quad= (\hat{\mathbf{e}}^R_{LO1}|V_1)(\hat{\mathbf{e}}^L_{LO2}|V_2)(\hat{\mathbf{e}}^{H'}_{LO3}|V_3)(\hat{\mathbf{e}}^{45^\circ}_{LO4}|V_4)\\
&\qquad+ (\hat{\mathbf{e}}^R_{LO1}|H_1)(\hat{\mathbf{e}}^L_{LO2}|H_2)(\hat{\mathbf{e}}^{H'}_{LO3}|H_3)(\hat{\mathbf{e}}^{45^\circ}_{LO4}|H_4)\\
&\quad\propto (\hat{\mathbf{e}}^R_{LO1},\hat{\mathbf{e}}^L_{LO2},\hat{\mathbf{e}}^{H'}_{LO1}|\Psi^3_{GHZ})_{cl},
\end{aligned} \tag{29}$$

where the contribution from the LO4 is a constant factor, since $(\hat{\mathbf{e}}^{45^\circ}_{LO4}|V_4) = 1/\sqrt{2}$ and $(\hat{\mathbf{e}}^{45^\circ}_{LO4}|H_4) = 1/\sqrt{2}$.

In this case, the magnitude of the signal $\gamma_{300\ \mathrm{kHz}}$ is proportional to the projection $\langle R_1L_2H'_3|\Psi^3_{GHZ}\rangle$. This is readily determined from Eq. (9) and indicates the existence of a classical signal corresponding to the element of reality $R_1L_2H'_3$ in the $Y_1Y_2X_3$ configuration as shown in Fig. 4(a) where a large signal amplitude is observed. However, when the LO3 polarization state is changed to V', this induces a minus sign in Eq. (29). Hence the magnitude of the signal $\gamma_{300\ \mathrm{kHz}}$ for the projection $(\hat{\mathbf{e}}^R_{LO1},\hat{\mathbf{e}}^L_{LO2},\hat{\mathbf{e}}^{V'}_{LO3}|\Psi^3_{GHZ})_{cl}$ is approximately zero as shown in Fig. 4(b). This signal is proportional to the projection $\langle R_1L_2V'_3|\Psi^3_{GHZ}\rangle = 0$ from Eq. (9) and so indicates that the element $R_1L_2V'_3$ in the *YYX* configuration is zero as predicted by GHZ entanglement. Similarly, the elements of reality $R_1R_2V'_3$, $L_1R_2H'_3$, and $L_1L_2V'_3$ in the $Y_1Y_2X_3$ configuration are nonzero as predicted by GHZ entanglement. The elements of reality not predicted by GHZ entanglement are $R_1R_2H'_3$, $L_1R_2V'_3$, and $L_1L_2H'_3$, respectively. The corresponding nonzero and zero classical-field state projections are given by Eq. (9):

$$\begin{aligned}
&(\hat{\mathbf{e}}^R_{LO1},\hat{\mathbf{e}}^L_{LO2},\hat{\mathbf{e}}^{H'}_{LO3}|\Psi^3_{GHZ})_{cl} \propto \langle R_1L_2H'_3|\Psi^3_{GHZ}\rangle = \frac{1}{2},\\
&(\hat{\mathbf{e}}^R_{LO1},\hat{\mathbf{e}}^L_{LO2},\hat{\mathbf{e}}^{LO3}_{V'}|\Psi^3_{GHZ})_{cl} \propto \langle R_1L_2V'_3|\Psi^3_{GHZ}\rangle = 0,\\
&(\hat{\mathbf{e}}^L_{LO1},\hat{\mathbf{e}}^R_{LO2},\hat{\mathbf{e}}^{H'}_{LO3}|\Psi^3_{GHZ})_{cl} \propto \langle L_1R_2H'_3|\Psi^3_{GHZ}\rangle = \frac{1}{2},\\
&(\hat{\mathbf{e}}^L_{LO1},\hat{\mathbf{e}}^R_{LO2},\hat{\mathbf{e}}^{V'}_{LO3}|\Psi^3_{GHZ})_{cl} \propto \langle L_1R_2V'_3|\Psi^3_{GHZ}\rangle = 0,\\
&(\hat{\mathbf{e}}^R_{LO1},\hat{\mathbf{e}}^R_{LO2},\hat{\mathbf{e}}^{V'}_{LO3}|\Psi^3_{GHZ})_{cl} \propto (R_1R_2V'_3|\Psi^3_{GHZ}\rangle = \frac{1}{2},\\
&(\hat{\mathbf{e}}^R_{LO1},\hat{\mathbf{e}}^R_{LO2},\hat{\mathbf{e}}^{H'}_{LO3}|\Psi^3_{GHZ})_{cl} \propto (R_1R_2H'_3|\Psi^3_{GHZ}\rangle = 0,\\
&(\hat{\mathbf{e}}^L_{LO1},\hat{\mathbf{e}}^L_{LO2},\hat{\mathbf{e}}^{V'}_{LO3}|\Psi^3_{GHZ})_{cl} \propto \langle L_1L_2V'_3|\Psi^3_{GHZ}\rangle = \frac{1}{2},\\
&(\hat{\mathbf{e}}^L_{LO1},\hat{\mathbf{e}}^L_{LO2},\hat{\mathbf{e}}^{H'}_{LO3}|\Psi^3_{GHZ})_{cl} \propto \langle L_1L_2H'_3|\Psi^3_{GHZ}\rangle = 0.
\end{aligned} \tag{30}$$

As shown in Fig. 4, the amplitude of the signal at 300 kHz, $\gamma_{300\ \mathrm{kHz}}$, has nonzero and zero amplitudes as predicted by Eq. (30), which are identical to the results for the corresponding quantum state.

The set of eight elements of reality for the *YYX* configuration is a complete set spanning the product basis for the polarization of the three measured fields, since a complete two-state basis is provided for each field. Hence, the total joint intensity at 300 kHz is contained in the eight possible elements for this configuration. Thus, for each element in this configuration, the classical joint intensity is normalized by dividing the absolute square of the signal amplitude $\gamma_{300\ \mathrm{kHz}}$ of each element of reality by the sum of the absolute squares of $\gamma_{300\ \mathrm{kHz}}$ for each element. The classical-field measurements then yield the joint probability representation of the *YYX* configuration which is shown in Fig. 4(i). Note, for comparison, that the predictions of quantum mechanics would yield a probability of $1/4 = 0.25$ for each large signal and zero for each small signal, showing that the classical joint intensities are in good agreement.

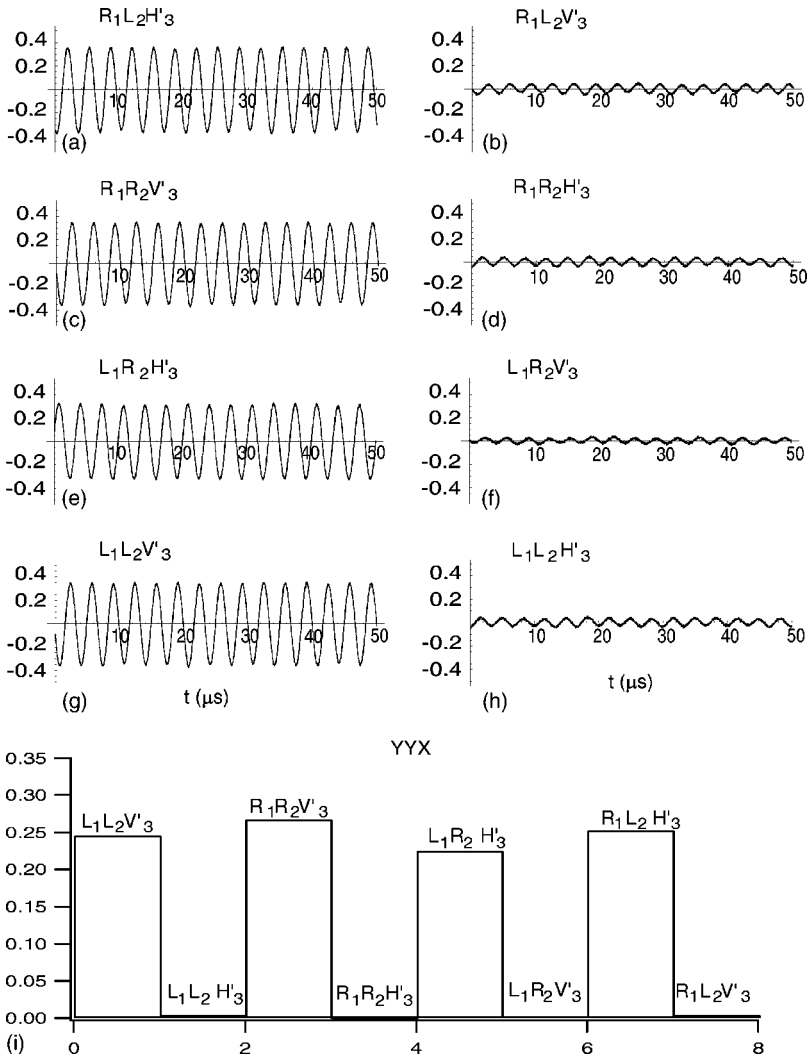

FIG. 4. Measurement of elements of reality for the *YYX* configuration using a four-classical-field entangled state. (a)(c)(e)(g) Components of physical reality predicted by GHZ entanglement exhibit nonzero signals at 300 kHz. (b)(d)(f)(h) Elements of physical reality not predicted by GHZ entanglement produce nearly zero signal at 300 kHz. (i) The normalized signal squared obtained for these elements agrees with the predictions of quantum mechanics.

Similarly, the measurements for the *YXY* and *XYY* configurations are shown in Figs. 5 and 6, demonstrating that the classical joint intensities are in agreement with the quantum predictions as they should be.

B. Measurement of the *XXX* configuration

Finally, we reproduce the polarization correlations for measurements for the $X_1X_2X_3$ configuration of three-particle GHZ entanglement which contradicts the theory of local realism. The appropriate polarization states of the local oscillator beams LO1, LO2, and LO3 are given by

$$\hat{\mathbf{e}}_{LO1}^{H',V'} = \frac{1}{\sqrt{2}}(\hat{H}_1 \pm \hat{V}_1),$$

$$\hat{\mathbf{e}}_{LO2}^{H',V'} = \frac{1}{\sqrt{2}}(\hat{H}_2 \pm \hat{V}_2), \tag{31}$$

$$\hat{\mathbf{e}}_{LO3}^{H',V'} = \frac{1}{\sqrt{2}}(\hat{H}_3 \pm \hat{V}_3).$$

For the eight combinations of linear polarizations in the *XXX*, the expected nonzero and zero classical-field state projections are given by

$$(\hat{\mathbf{e}}_{LO1}^{H'}, \hat{\mathbf{e}}_{LO2}^{H'}, \hat{\mathbf{e}}_{LO3}^{H'} | \Psi_{GHZ}^3)_{cl} \propto \langle H_1' H_2' H_3' | \Psi_{GHZ}^3 \rangle = \frac{1}{2},$$

$$(\hat{\mathbf{e}}_{LO1}^{V'}, \hat{\mathbf{e}}_{LO2}^{H'}, \hat{\mathbf{e}}_{LO3}^{H'} | \Psi_{GHZ}^3)_{cl} \propto \langle V_1' H_2' H_3' | \Psi_{GHZ}^3 \rangle = 0,$$

$$(\hat{\mathbf{e}}_{LO1}^{V'}, \hat{\mathbf{e}}_{LO2}^{V'}, \hat{\mathbf{e}}_{LO3}^{H'} | \Psi_{GHZ}^3)_{cl} \propto \langle V_1' V_2' H_3' | \Psi_{GHZ}^3 \rangle = \frac{1}{2},$$

$$(\hat{\mathbf{e}}_{LO1}^{H'}, \hat{\mathbf{e}}_{LO2}^{V'}, \hat{\mathbf{e}}_{LO3}^{H'} | \Psi_{GHZ}^3)_{cl} \propto \langle H_1' V_2' H_3' | \Psi_{GHZ}^3 \rangle = 0,$$

$$(\hat{\mathbf{e}}_{LO1}^{H'}, \hat{\mathbf{e}}_{LO2}^{V'}, \hat{\mathbf{e}}_{LO3}^{V'} | \Psi_{GHZ}^3)_{cl} \propto \langle H_1' V_2' V_3' | \Psi_{GHZ}^3 \rangle = \frac{1}{2},$$

$$(\hat{\mathbf{e}}_{LO1}^{V'}, \hat{\mathbf{e}}_{LO2}^{V'}, \hat{\mathbf{e}}_{LO3}^{V'} | \Psi_{GHZ}^3)_{cl} \propto \langle V_1' V_2' V_3' | \Psi_{GHZ}^3 \rangle = 0,$$

$$(\hat{\mathbf{e}}_{LO1}^{V'}, \hat{\mathbf{e}}_{LO2}^{H'}, \hat{\mathbf{e}}_{LO3}^{V'} | \Psi_{GHZ}^3)_{cl} \propto \langle V_1' H_2' V_3' | \Psi_{GHZ}^3 \rangle = \frac{1}{2},$$

$$(\hat{\mathbf{e}}_{LO1}^{H'}, \hat{\mathbf{e}}_{LO2}^{H'}, \hat{\mathbf{e}}_{LO3}^{V'} | \Psi_{GHZ}^3)_{cl} \propto \langle H_1' H_2' V_3' | \Psi_{GHZ}^3 \rangle = 0. \tag{32}$$

For the eight possible measurements in the *XXX* configuration, the zero and nonzero signal amplitudes $\gamma_{300\ \mathrm{kHz}}$ for each element of reality with $X_1X_2X_3 = \pm 1$ are shown in Fig. 7. For the elements of reality with $X_1X_2X_3 = -1$, i.e., $H_1'H_2'V_3'$,

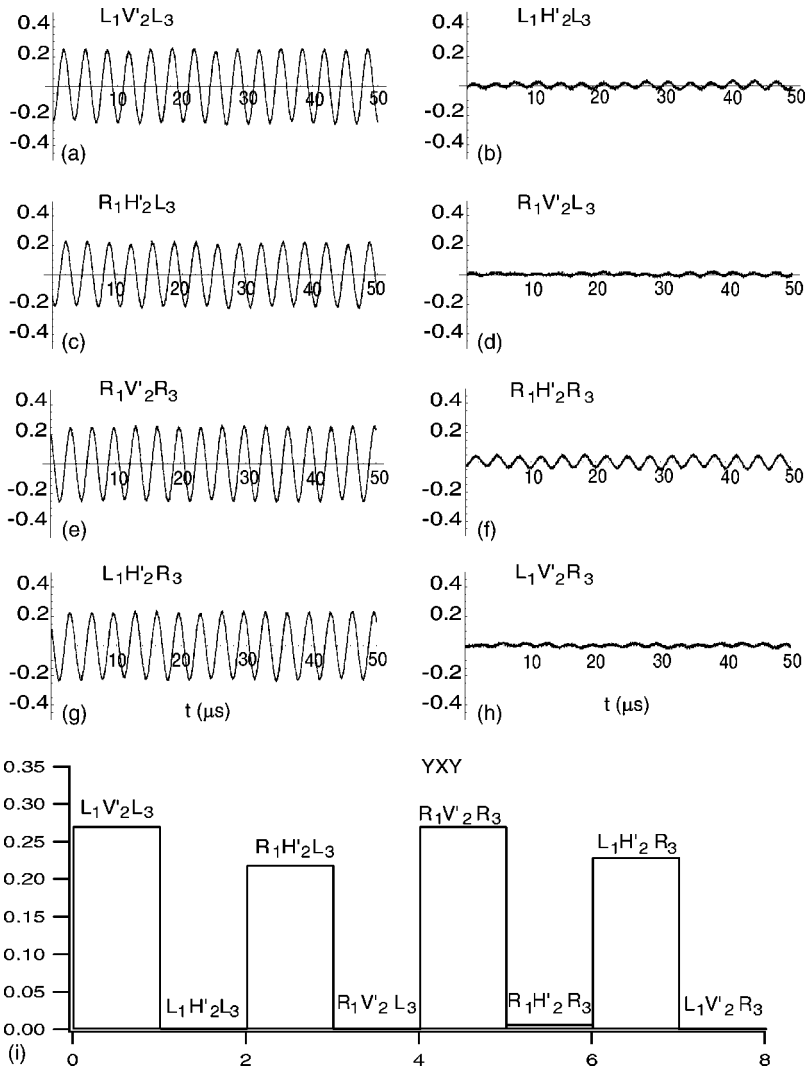

FIG. 5. Measurement of elements of reality for the *YXY* configuration using a four-classical-field entangled state. (a),(c),(e),(g) Components of physical reality predicted by GHZ entanglement exhibit nonzero signals at 300 kHz. (b),(d),(f),(h) Elements of physical reality not predicted by GHZ entanglement produce nearly zero signal at 300 kHz. (i) The normalized signal squared obtained for these elements agrees with the predictions of quantum mechanics.

$V_1'V_2'V_3'$, $H_1'V_2'H_3'$, and $V_1'H_2'H_3'$, the signal amplitude $\gamma_{300\ \mathrm{kHz}}$ is zero. For the elements of reality with $X_1X_2X_3=+1$, i.e., $V_1'H_2'V_3'$, $H_1'V_2'V_3'$, $V_1'V_2'H_3'$, and $H_1'H_2'H_3'$, the signal amplitude $\gamma_{300\ \mathrm{kHz}}$ is nonzero. The normalized joint intensity representation of the classical signals for the *XXX* configuration is also shown in Fig. 7(i).

The experimental observations for the $X_1X_2X_3$ configuration produced by our classical-wave system are in agreement with the quantum predictions of GHZ entanglement, giving strong signals only when $X_1X_2X_3=+1$. Our experiments formally produce results which contradict the predictions of local realism, where strong signals are expected only if $X_1X_2X_3=-1$. By reproducing the 32 elements of the truth table, we have demonstrated that the entangled four-classical-field state exhibits the same polarization correlations as in the quantum system. Since particle properties are not required for reproducing the correlations, this result is a consequence of reproducing all of the superposition and interference properties of the corresponding quantum state.

VI. ENTANGLEMENT SWAPPING

The classical-field scheme is readily modified to demonstrate a form of entanglement swapping [25]. In our experiments, all four beams are not entangled prior to joint heterodyne detection and frequency selection. Hence, the input state effectively corresponds to noninteracting particles. We can arrange for an observer A to make a type of Bell state measurement on beams 1 and 2. Observer A transmits a classical signal to another observer B who measures polarization correlations for beams 3 and 4. By multiplying the classical signal from observer A by his signal and band pass filtering at 300 kHz, observer B observes correlations corresponding to the Bell state selected by observer A. This method works by a form of generalized two-frequency phase-sensitive detection and reproduces the correlations present in $|\Psi_{GHZ}^4)_{cl}$ as described below.

In this method, seen in Fig. 8, the symmetrical detection diagram of Fig. 3 is used for beams 1 and 2, measured by observer A and for beams 3 and 4, measured by observer B. Observer A multiplies the signals from a pair of detectors 1 and 2, band passes the product signal at 60 and 240 kHz and then sums. Defining horizontal (H) and vertical (V) field components, this yields from beams 1 and 2 a signal amplitude $S_{12}(t)\propto(\hat{\mathbf{e}}_{LO1}\hat{\mathbf{e}}_{LO2}|\Phi_+(t))_{12}$, where $|\Phi_+(t))_{12}$ is a time-dependent Bell state, $|\Phi_+(t))_{12}=[|H_1H_2)\exp(2i\delta_Ht)+|V_1V_2)\exp(2i\delta_Vt)]/\sqrt{2}$, with $2\delta_H=2\pi\times 60$ kHz, and $2\delta_V$

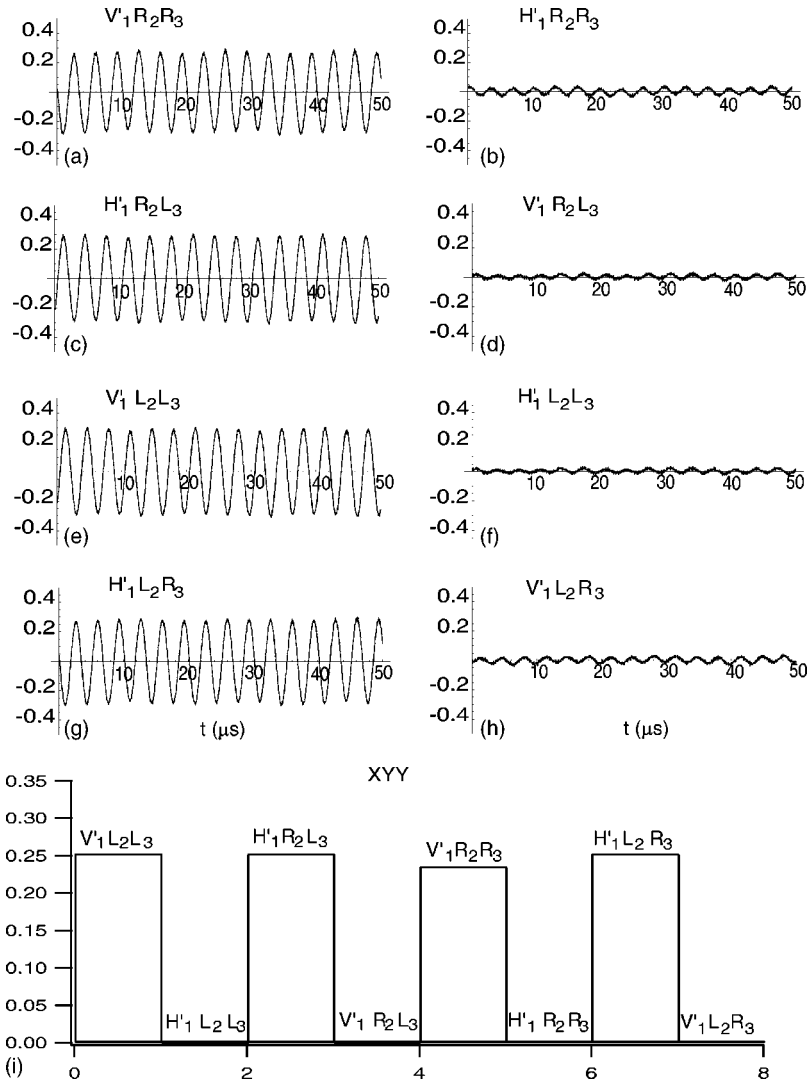

FIG. 6. Measurement of elements of reality for the *XYY* configuration using a four-classical field entangled state. (a),(c),(e),(g) Components of physical reality predicted by GHZ entanglement exhibit nonzero signals at 300 kHz. (b),(d),(f),(h) Elements of physical reality not predicted by GHZ entanglement produce nearly zero signal at 300 kHz. (i) The normalized signal squared obtained for these elements agrees with the predictions of quantum mechanics.

$=2\pi\times 240$ kHz. Observer B does the same for beams 3 and 4, where the horizontal and vertical components are interchanged with respect to beams 1 and 2, yielding a signal amplitude $S_{34}(t)\propto(\hat{\mathbf{e}}_{LO3}\hat{\mathbf{e}}_{LO4}|\Phi_+(t))_{34}$, where $|\Phi_+(t))_{34}=[|V_3V_4)\exp(2i\delta_H t)+|H_3H_4)\exp(2i\delta_V t)]/\sqrt{2}$. Multiplying the signals corresponding to S_{12} and S_{34} together in a third analog multiplier and bandpassing at 300 kHz yields two interfering contributions proportional to the inner products of the four LO polarizations with $|\Psi^4_{GHZ})_{cl}=[|H_1H_2H_3H_4)+|V_1V_2V_3V_4)]/\sqrt{2}$ as before.

In order to demonstrate classical-field entanglement swapping, we imagine that observer A sets his local oscillator polarizations at 45°, and measures $S_{12}(t)$. Observer A sends his signal to observer B who measures $S_{34}(t)$ for arbitrary LO3 and LO4 polarizations. Observer B multiplies his signal by the signal sent from observer A and band passes the product signal at 300 kHz. As described above, the signal at 300 kHz is proportional to the inner product of the four LO polarizations with $|\Psi^4_{GHZ})_{cl}$. Since observer A has fixed LO polarizations at 45°, observer B measures polarization correlations characteristic of the time-independent Bell state $|\Phi_+)_{34}=[|H_3H_4)+|V_3V_4)]/\sqrt{2}$. If observer A sets his LO1 polarization at 45° and his LO2 polarization at −45°, then observer B measures polarization correlations corresponding to the Bell state $|\Phi_-)_{34}=[|H_3H_4)-|V_3V_4)]/\sqrt{2}$. As in the quantum case, only certain Bell states can be swapped [25]. It is necessary to change the experimental set up to swap other Bell states, such as $[|H_3V_4)\pm|V_3H_4)]/\sqrt{2}$.

In our experiments, with the polarizations of observer A set to 45°, 45°, respectively, we find that observer B obtains a nonzero signal at 300 kHz when his polarizers are set to 45°, 45°, and a zero signal when his polarizers are set to 45°, −45°, respectively, as shown in Fig. 9. This corresponds to measurement of the Bell state $|\Phi_+)_{34}$ for observer B as it should. This result shows that observer A can generate a classical signal which controls the entangled state which will be observed by B.

VII. DISCUSSION

In this paper, we have shown that multiplication of signals obtained by heterodyne detection of classical fields can be used to measure classical-field correlations, which correspond to entangled states. The squared magnitude of the product signal is the joint intensity in the classical experiments. Entangled states are selected by postprojection using

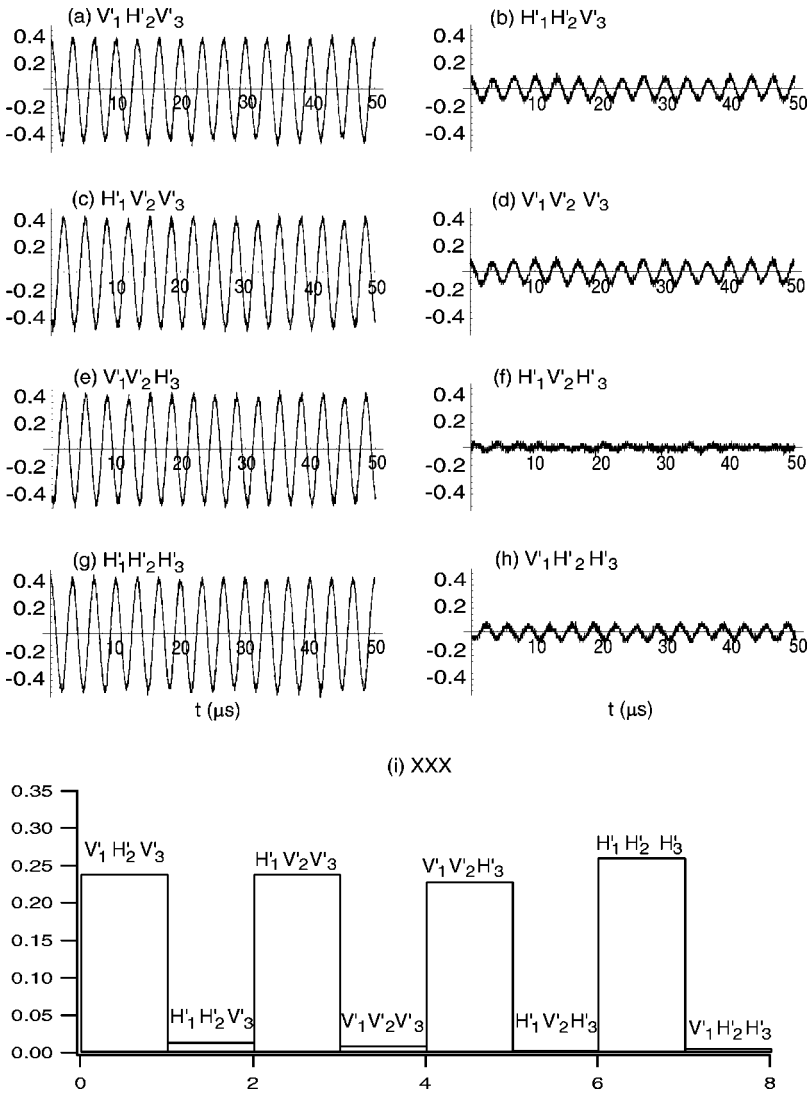

FIG. 7. Demonstrating violation of local realism theory by measurement of elements of reality for the *XXX* configuration using a four-classical-field state. (a),(c),(e),(g) Elements of physical reality predicted by GHZ entanglement exhibit nonzero signals at 300 kHz. (b),(d),(f),(h) Elements of physical reality not predicted by GHZ entanglement produce nearly zero signal at 300 kHz. (i) The normalized signal squared obtained for these elements agrees with the predictions of quantum mechanics producing strong signals only when $XXX=1$, i.e., for $V_1'H_2'V_3'$, etc. This is in contradiction with local realism which predicts strong signals only when $XXX=-1$, i.e., for $H_1', H_2'V_3'$, etc.

frequency domain band pass methods, rather than time domain coincidence detection as in photon counting experiments. Classical postselection is implemented after combining heterodyne detection signals from spatially separated observers. This is different from the quantum case where the postselection technique can be implemented by any of the independent observers. Our postselection is only possible after the independent observers combine their data and then select the desired frequency components. This biased statistical analysis permits classical fields or photons from independent sources to exhibit nonclassical correlations.

In our experiments, the nonlocal correlations of a four-particle entangled state are reproduced by using a simple scheme employing heterodyne detection of four classical fields, yielding large robust signals which are independent of the phases of the local oscillators. The correlations for the classically entangled four-field state are demonstrated by formally reproducing the 32 elements of the truth table obtained in a three-particle quantum GHZ experiment on the violation of local realism.

We have given a simple argument to show that intensity correlations in low count rate quantum experiments can be considered to arise from correlated fields. The correlated field fluctuations can be directly measured by multiplying balanced homodyne detection signals. The squared magnitude of this correlated field signal reproduces the joint probabilities obtained in the corresponding intensity correlation experiments and is closely related to the classical joint intensity measured in our classical-field experiments.

The classical-field experiments differ from their photon counting quantum counterparts in that they fail to exhibit the wave-particle duality of the quantum experiments: Only the interference features are reproduced. However, since the classical-field state is directly measured, the classical experiments are similar to quantum experiments, which use homodyne detection methods [16–18].

The ability to generate entangled states of many particles is essential to the development of quantum information processing methods. Generation of such states can be very challenging in real quantum systems, where loss and decoherence easily destroy the state and coincidence count rates tend to be low when the number of particles is large. The production of a classically entangled four-field state may serve as a first step in developing classical-wave methods to simulate a

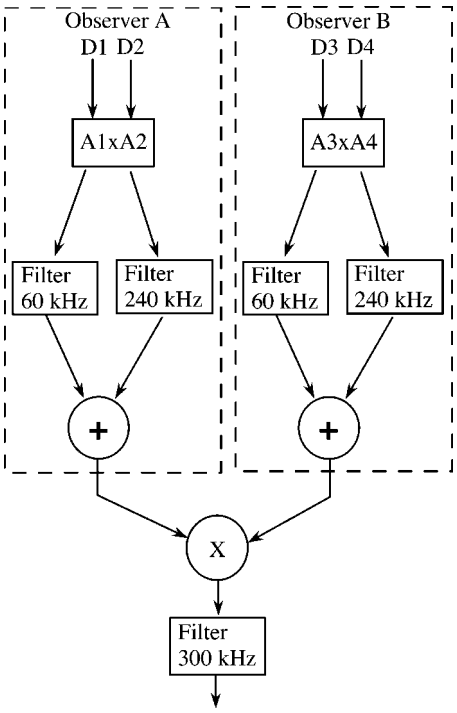

FIG. 8. Symmetrical detection scheme for demonstrating classical-field entanglement swapping in the four-field basis. The signal measured by observer A is sent to observer B, who multiplies this signal by his own to obtain a net signal at 300 kHz. Observer B then measures correlations determined by the Bell state chosen by observer A.

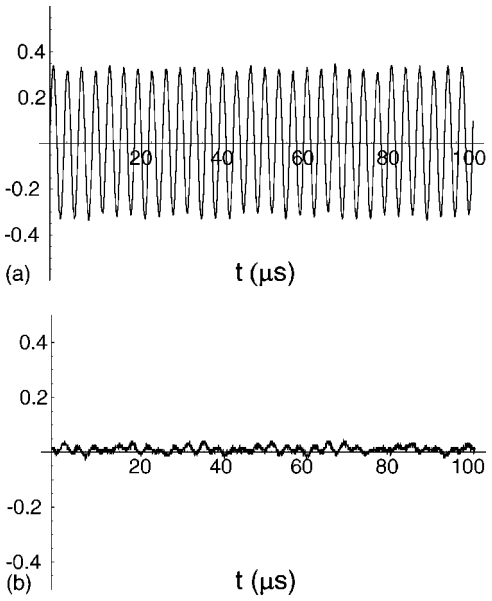

FIG. 9. Demonstration of entanglement swapping. Observer A sets his LO 1 and 2 polarizations at 45° and 45°, respectively, to select the Bell state $|\phi_{cl}^{+})_{12}$. Observer B's signals are then proportional to the projections of the corresponding Bell state $|\phi_{cl}^{+})_{34}$ onto the polarizations of LO's 3 and 4. (a) Observer B sets his LO 3 and 4 polarizations at 45° and 45°, respectively, yielding a nonzero signal at 300 kHz. (b) Observer B sets his LO 3 and 4 polarizations at 45° and −45°, respectively, yielding a zero signal at 300 kHz.

quantum network. The demonstration of a classical form of entanglement swapping in the four-field basis is already a type of information processing, as it enables the correlation measurements of one observer to determine the correlation measurements for another observer. Scaling in the classical-field method is a concern [1]. However, producing the maximally entangled state of 2^N particles never requires more than two input frequencies and two band-pass filters, as in the present experiments.

We note that to measure correlations between separated beams, the classical scheme employs four independent, spatially separated LO beams. In principle, the signal from each heterodyne detector can be recorded and correlated at a later time. This is possible since the relative phases of all of the pairs of superposed fields are preserved in propagation to the detectors. The signals can then be analyzed numerically, using multiplication and appropriate frequency selection. For this scheme to work, it is necessary that the four observers synchronize their time origins with a precision small compared to the inverse of the frequency differences employed in the experiments. This can be accomplished with a light pulse from the source region to all observers. In the quantum experiments, the observers must be sure to measure correlated photons produced in the same event. For low count rates, this is readily assured: if the experiment produces only one repetition per hour, it is easy for the observers to synchronize the measurement timing. Of course, an important goal of current quantum experiments is to achieve very high repetition rates. As the rate increases, the observers must choose time origins which are consistent within the inverse of the production rate of correlated photons.

The classical-field correlation experiments exhibit many features which are in common their quantum counterparts. The unitary evolution of a pure quantum state and the evolution of the classical field are both deterministic, although the quantum measurements are not. The calculation of the projections of the classically entangled field states is identical to that of the quantum counterpart, reproducing the multiparticle interferences and the corresponding polarization correlations. Except for the nonlinear elements in the quantum sources, both systems employ nearly identical linear optical networks for combining beams and for detection. The number of analog multipliers used in the classical correlation measurements is identical to the number of multiplications required in the corresponding quantum coincidence measurements. Quantum correlation experiments often employ postprojection based on coincidence counting [3]. In our classical scheme, postprojection is accomplished by a frequency filtering method that enables selection of the desired components of the multiparticle wavefunction, although this occurs after combining the data of the multiple observers. As in the quantum experiments, the implementation of four-particle entanglement is easier than for three-particles: To directly simulate a three particle entangled state, three frequencies are required. By contrast, only two frequencies and three beamsplitters are required to generate an output that simulates four-particle entanglement, because the polarizations can be interchanged in pairs. This is similar to the use of two

pairs of parametric down converters in the corresponding quantum mechanical experiments. As in the classical experiments, it is easier to demonstrate three-particle quantum GHZ entanglement starting from a four-particle entangled state by using the fourth photon as a trigger. In demonstrat ing a form of entanglement swapping, we find a limitation in the basis of Bell states that can be swapped without changing the experimental configuration. This is similar to the limitation encountered in the quantum experiments [25].

ACKNOWLEDGMENT

This research was supported by the National Science Foundation.

[1] R. J. C. Spreeuw, Phys. Rev. A **63**, 062302 (2001).
[2] K. F. Lee, F. Reil, S. Bali, A. Wax, and J. E. Thomas, Opt. Lett. **24**, 1370 (1999).
[3] Z. Y. Ou and L. Mandel, Phys. Rev. Lett. **61**, 50 (1988).
[4] Z. Y. Ou, S. F. Pereira, H. J. Kimble, and K. C. Peng, Phys. Rev. Lett. **68**, 3663 (1992).
[5] R. Somma, G. Ortiz, H. Barnum, E. Knill, and L. Viola, Bull. Am. Phys. Soc. **48**, 993 (2003).
[6] N. J. Cerf, C. Adami, and P. G. Kwiat, Phys. Rev. A **57**, R1477 (1998).
[7] E. Knill, R. Laflamme, and G. J. Milburn, Nature (London) **409**, 46 (2001).
[8] C. Elliot, New J. Phys. **4**, 46 (2002).
[9] D. Stucki, N. Gisin, O. Guinnard, G. Ribordy, and H. Zbinden, New J. Phys. **4**, 46 (2002).
[10] T. B. Pittman, M. J. Fitch, B. C. Jacobs, and J. D. Franson, Phys. Rev. A **68**, 032316 (2003).
[11] T. B. Pittman, B. C. Jacobs, and J. D. Franson, Phys. Rev. A **66**, 052305 (2002).
[12] T. B. Pittman, B. C. Jacobs, and J. D. Franson, Phys. Rev. A **64**, 062311 (2001).
[13] T. C. Ralph, W. J. Munro, and R. E. S. Polkinghorne, Phys. Rev. Lett. **85**, 2035 (2000).
[14] A. Peres, in *Potentiality, Entanglement and Passion-at-a-Distance*, edited by R. S. Cohen, M. Horne, and J. J. Stachel (Kluwer Academic, Dordrecht, 1997), pp. 191–196.
[15] Z. Y. Ou, S. F. Pereira, H. J. Kimble, and K. C. Peng, Phys. Rev. Lett. **68**, 3663 (1992).
[16] P. Grangier, M. J. Potasek, and B. Yurke, Phys. Rev. A **38**, 3132 (1988).
[17] A. Kuzmich, I. A. Walmsley, and L. Mandel, Phys. Rev. Lett. **85**, 1349 (2000).
[18] A. Kuzmich, I. A. Walmsley, and L. Mandel, Phys. Rev. A **64**, 063804 (2001).
[19] K. F. Lee and J. E. Thomas, Phys. Rev. Lett. **88**, 097902 (2002).
[20] R. J. C. Spreeuw, Found. Phys. **28**, 361 (1998).
[21] J. W. Pan, D. Boumeester, M. Daniell, H. Wienfurter, and A. Zeilinger, Nature (London) **65**, 032321 (2002).
[22] D. M. Greenberger, M. A. Horne, A. Shimony, and A. Zeilinger, Am. J. Phys. **58**, 1131 (1990).
[23] D. T. Smithey, M. Beck, M. G. Raymer, and A. Faridani, Phys. Rev. Lett. **70**, 1244 (1993).
[24] D. Boumeester, J. W. Pan, M. Daneiell, H. Weinfurter, and A. Zeilinger, Phys. Rev. Lett. **82**, 1345 (1999).
[25] J. W. Pan, M. Daniell, S. Gasparoni, G. Weihs, and A. Zeilinger, Phys. Rev. Lett. **86**, 4435 (2001).